AUTHOR QUERY FORM

Dear Author,

Please check your proof carefully and mark all corrections at the appropriate place in the proof (e.g., by using on-screen annotation in the PDF file) or compile them in a separate list. Note: if you opt to annotate the file with software other than Adobe Reader then please also highlight the appropriate place in the PDF file. To ensure fast publication of your paper please return your corrections within 48 hours.

For correction or revision of any artwork, please consult http://www.elsevier.com/artworkinstructions.

Any queries or remarks that have arisen during the processing of your manuscript are listed below and highlighted by flags in the proof.

Location in article	Query / Remark: Click on the Q link to find the query's location in text Please insert your reply or correction at the corresponding line in the proof
Q1	As per the journal style , the section heading "Introduction" is mandatory. Kindly provide the same.
Q2	Please check the footnotes in Table 3 and change if necessary.
Q3	Please confirm that given names and surnames have been identified correctly. Please check this box or indicate your approval if you have no corrections to make to the PDF file ☐

Thank you for your assistance.

Graphical abstract

Solid State Sci. **2013**, ■, ■ ■ ■

In situ study of the formation of rhenium borides from the elements at high-(*p, T*) conditions: Extreme incompressibility of Re₇B₃ and formation of new phases

Erick A. Juarez-Arellano [a,*], Björn Winkler [b], Alexandra Friedrich [b], Lkhamsuren Bayarjargal [b], Wolfgang Morgenroth [b], Martin Kunz [c], Victor Milman [d]

[a] *Instituto de Química Aplicada, Universidad del Papaloapan, Circuito Central 200, Parque Industrial, 68301 Tuxtepec, Oaxaca, Mexico*

Schematic *p–T* field of the phases observed during the reaction of rhenium and boron from the elements in a laser heated diamond anvil cell. The formation of at least two new phase (called phase A and phase B) was observed. The lines are only guides to the eye.
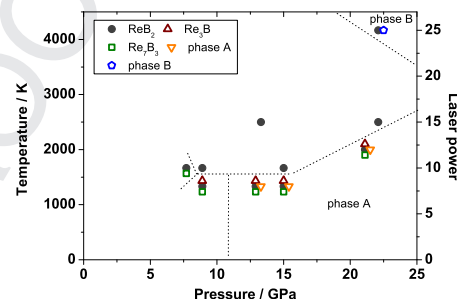
In situ study of the formation of rhenium borides from the elements at high-(p, T) conditions: Extreme incompressibility of Re_7B_3 and formation of new phases

Q3 Erick A. Juarez-Arellano [a],*, Björn Winkler [b], Alexandra Friedrich [b], Lkhamsuren Bayarjargal [b], Wolfgang Morgenroth [b], Martin Kunz [c], Victor Milman [d]

[a] Instituto de Química Aplicada, Universidad del Papaloapan, Circuito Central 200, Parque Industrial, 68301 Tuxtepec, Oaxaca, Mexico
[b] Institut für Geowissenschaften, Goethe-Universität Frankfurt, Altenhöferallee 1, 60438 Frankfurt a.M., Germany
[c] Advanced Light Source, Lawrence Berkeley National Laboratory, 1 Cyclotron Road, Berkeley, CA 94720, USA
[d] Accelrys, 334 Science Park, Cambridge, UK

A B S T R A C T

Based on in situ synchrotron X-ray diffraction experiments employing laser heated diamond anvil cells to investigate the reaction of rhenium and boron from the elements at high-(p, T) conditions, Re_7B_3 was found to be extremely incompressible, with $B_{Re_7B_3} = 435(14)$ GPa, making it one of the least compressible binary compounds known to date. We also have determined the previously unknown bulk modulus of Re_3B, $B_{Re_3B} = 320(15)$ GPa, and have confirmed earlier reports of the bulk modulus of ReB_2, $B_{ReB_2} = 360(18)$ GPa. The experimental findings were supported by density functional theory calculations, which were also employed to compute elastic stiffness coefficients and estimates for the hardness. At different high-(p, T) conditions the formation of new phases were observed.

© 2013 Elsevier Masson SAS. All rights reserved.

Transition metal borides, TM-borides, are a large family of compounds many of which have outstanding physical properties, such as the high bulk modulus of OsB (453 GPa [1]), or the ultra-hardness of ReB_2 (Hv = 30–48 GPa [1,2]) and WB_4 (Hv = 46 GPa [1]). Hence, TM-borides have been studied extensively both theoretically and experimentally; and most are well characterized at ambient conditions and high temperatures (e.g. Refs. [3–6]). The synthesis of most TM-borides at ambient pressure is relatively straightforward and can be achieved by heating a mixture of the elements above ≈1500 K in air. All transition metals from periods 4–6 with the exception of Cd and Hg have been shown to form binary borides [7]. In contrast to the numerous ambient pressure studies and very many theoretical high pressure studies, compara-

Q1 tively few in situ high pressure studies have been presented [8–15].

Rhenium diboride, ReB_2, is one of the most studied TM-borides due to its hardness and incompressibility. Investigations are favored by the fact that it can be synthesized at ambient pressure

[16]. Several synthesis methods have been employed to obtain ReB_2 as powder, single crystals or as thin films, including solid state reactions, self-propagating high-temperature synthesis, arc melting, zone melting, floating zone furnace-based techniques and pulsed laser deposition, among others [2,16–19]. In contrast, the other two binary phases that have been observed in the Re–B system, namely Re_3B and Re_7B_3 have attracted much less attention [20,21]. Kawano et al. [22] reported the superconductivity of Re_7B_3 (T_c = 3.3 K) and Re_3B (T_c = 4.8 K), while Takagiwa et al. [23] reported the magnetic properties of Re_3B. Phase stabilities at high-(p, T) conditions are currently unknown in the Re–B system and the compressibilities of Re_3B and Re_7B_3 have not been determined yet. No in situ high pressure synthesis studies of rhenium borides have been reported up to now.

In the present study we therefore explore the reaction of rhenium and boron by in situ experiments to understand processes occurring at high-pressures and high temperatures using laser-heated diamond anvil cell experiments. We have also determined the compressibilities of the rhenium borides and discuss our findings by comparing the experimental results to those obtained by density functional theory (DFT) based atomistic model calculations in the present study and by other authors [24–32].

* Corresponding author. Tel.: +52 28787 59240x220; fax: +52 28787 59240x230.
E-mail addresses: eajuarez@unpa.edu.mx, eradjuar@hotmail.com (E.A. Juarez-Arellano).

1. High-pressure X-ray diffraction

High pressure experiments were performed at the Advanced Light Source (ALS, Berkeley, USA, beamline 12.2.2). Small pieces of rhenium foil (Aldrich Chemical, purity 99.98%) with a thickness of 25 μm and boron powder (~325 mesh, Alpha Aesar, 98 %) were used as starting materials. Both materials had been characterized earlier [33,15]. The samples were pressurized in Boehler—Almax diamond anvil cells and were double sided laser heated with fiber lasers. NaCl and KCl were used as a pressure-transmitting medium and for thermal insulation. Gasket holes with diameters of ~140 μm were drilled by a home-built laser lathe through tungsten gaskets (preindented to 40 μm). Diffraction patterns were acquired with a MAR345 image plate detector using two different wavelengths of 0.4132 Å and 0.4959 Å. Patterns were collected both during and after laser heating. The sample-to-detector distance of 320.817 mm was determined from a LaB_6 reference sample. Counting times varied between 120 and 360 s. Most data collection was done with a 10×10 μm^2 FWHM beam spot. The laser spots had a diameter of about 30 μm. Due to technical problems with the temperature determination, only approximate temperatures could be determined. Laser heating with moderate laser power (around 8—15 W per laser) led to bright hot spots and temperatures of about 1400—2500 K in the sample. The optical emission of the samples which react on laser heating is very variable and a more reliable temperature determination was not possible. In all cases, before and after each exposure, pressure was determined by the laser-induced ruby-fluorescence technique, applying the pressure scale of Mao et al. [34].

Recovered samples were measured at ambient conditions at the beamline P02.2 of the PETRA III synchrotron (DESY Photon Science, Hamburg, Germany). Diffraction patterns were acquired using a wavelength of 0.2907 Å, a beam focused to 5×5 μm^2 full width at half maximum using Kirkpatrick—Baez mirrors and a PerkinElmer XRD1621 detector. The sample-to-detector distance of 750 mm was determined from a CeO_2 reference sample. All the diffraction images were processed, corrected for distortion and integrated using FIT2D [35]. The background of the integrated powder diffraction patterns was extracted using the program DATLAB [36]. Le Bail fits were performed using the program FULLPROF [37] in order to obtain unit cell parameters. A linear interpolation between approximately 30 manually selected points for the background and a pseudo-Voigt profile function were used.

2. Density functional theory based model calculations

In order to better understand the structure-property relations of our synthesis products, density functional theory (DFT) calculations were performed employing the CASTEP code [38]. The code is an implementation of Kohn-Sham DFT based on a plane wave basis set in conjunction with pseudopotentials. The plane wave basis set is unbiased (as it is not atom-centered) and does not suffer from basis—set superposition errors, unlike atom-centered basis sets. It also makes converged results straightforward to obtain in practice, as the convergence is controlled by a single adjustable parameter, the plane wave cut-off, which we set to 500—700 eV. All pseudopotentials were ultrasoft and were generated using the WC-GGA [39] to allow for a fully consistent treatment of the core and valence electrons. The Brillouin zone integrals were performed using Monkhorst—Pack grids [40] with spacings between grid points of less than 0.02 Å^{-1}. A simultaneous optimization of the unit cell parameters and internal co-ordinates was performed so that forces were converged to 0.005 eV/Å and the stress residual to 0.005 GPa. Elastic stiffness coefficients were obtained by stress-strain calculations. Based on the elastic stiffness coefficients

estimates of the Vickers microhardness Hv were computed according to the approach described by Ivanovskii [41].

3. Results and discussion

3.1. Phase stabilities

Typical powder X-ray diffraction patterns obtained at high pressure before any laser heating are shown in Fig. 1. KCl transforms from the B1($Fm\overline{3}m$) to the B2($Pm\overline{3}m$) structure type at around 2 GPa [42]. The X-ray powder diffraction patterns before laser heating can be completely indexed by assigning peaks to either rhenium or the pressure-transmitting medium used, B2—KCl or NaCl. Boron is not detectable due to its comparatively small X-ray scattering cross-section. We detected no influence of the pressure-transmitting medium on the results and therefore this aspect will not be discussed any further in the following.

The reaction of rhenium and boron at ~9 GPa was triggered by a brief irradiation with laser light at low laser power (8 W each laser, corresponding to a temperature of $T \sim 1500$ K). An analysis of the X-ray diffraction patterns obtained after laser heating showed the presence of ReB_2, Re_3B, Re_7B_3, and NaCl (Fig. 2a). Lattice parameters of the structures discussed here are summarized in Table 1. Increasing the laser power to 10 W for each laser at ~9 GPa yielded temperatures of ~1800 K. At these conditions ReB_2 becomes the
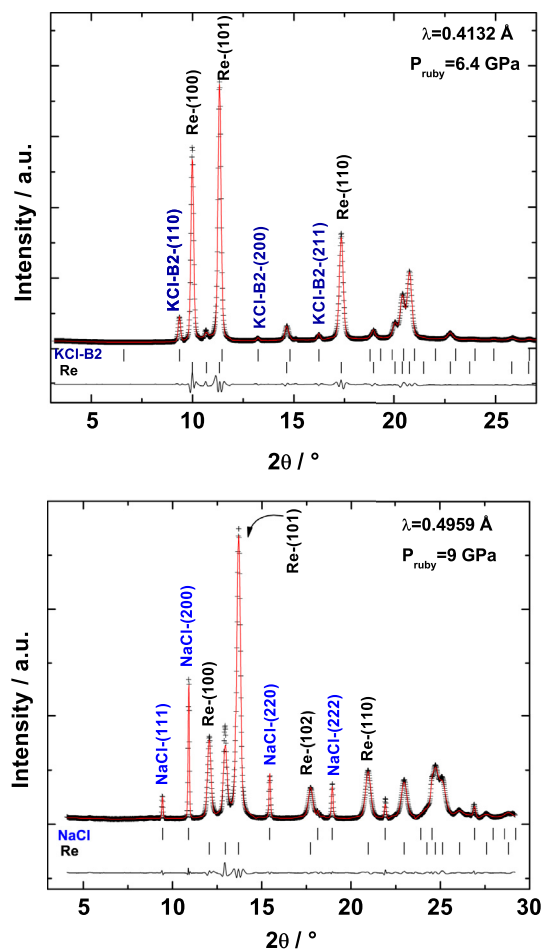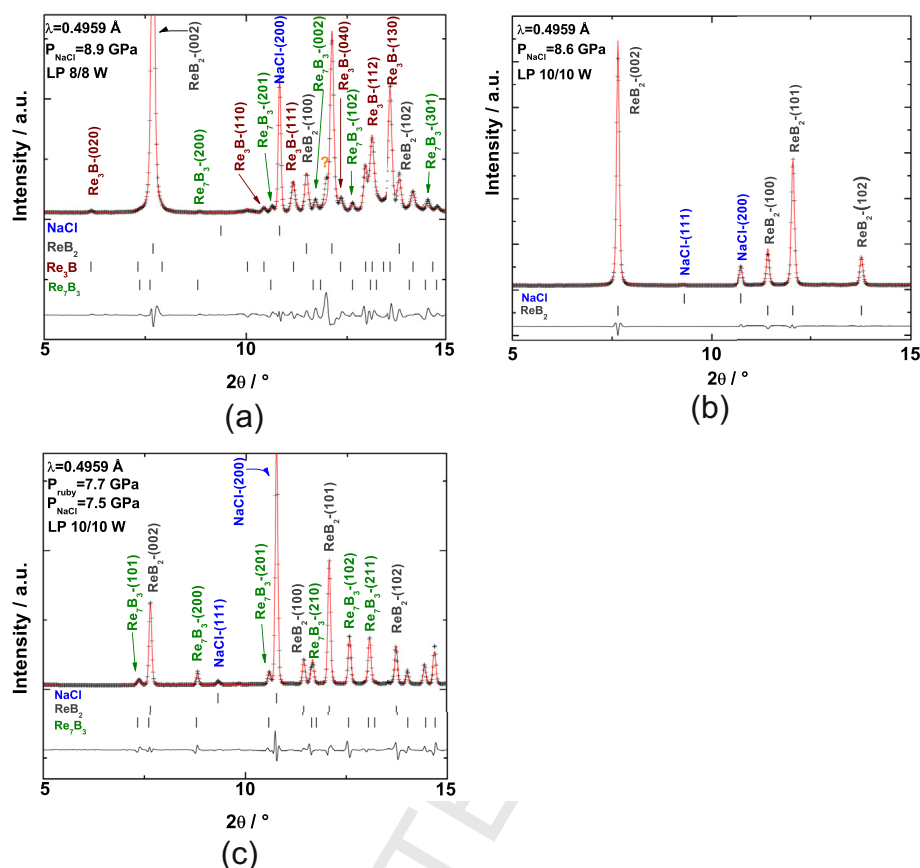

Fig. 1. Powder X-ray diffraction patterns recorded at high pressure before laser heating. The diffraction patterns before laser heating can be completely indexed by assigning peaks to either rhenium or the pressure-transmitting medium used, B2—KCl or NaCl.

Fig. 2. Powder X-ray diffraction patterns obtained after laser heating a mixture of rhenium and boron in a DAC. LP denotes the upstream and downstream laser power used. The enlargements of the X-ray diffraction patterns shows the good quality of the fit and the coexistence of different Re–B phases: ReB_2, Re_3B and Re_7B_3 (a, b, c) at different (p, T) conditions. Question marks indicate unindexed reflections.

stable phase (Fig. 2b) and the other rhenium boride phases disappear. If the pressure is slightly reduced to ~7.6 GPa while continuing to heat with this laser power, reflections due to the presence of Re_7B_3 reappear and the product is a mixture of ReB_2 and Re_7B_3 (Fig. 2).

Around 15 GPa and ~1500 K, the phases Re_7B_3, ReB_2 and Re_3B were present. It is not obvious, which of the phases are stable and which are metastable. In addition, a few new reflections were also detected (Fig. 3a). These extra reflections did not belong to any previously reported Re–B phase, to any high-pressure boron phase, or to any of the materials that may have some contributions in the diffraction pattern like the gasket, the ruby chips (for pressure measurements) or the diamonds. Therefore we assign them to a new Re–B phase. Attempts to index these new reflections failed due to their strong overlap with other reflections. However, for the sake of the discussion the new phase was called phase A.

After increasing the laser power to 15 W, so that sample temperatures were ~2500 K at ~13 GPa, the multiphase mixture disappears and we obtain a single phase, ReB_2 (Fig. 3b). At 21 GPa and 13 W laser power (~2000 K) we again observed ReB_2, Re_3B, Re_7B_3, and phase A (Fig. 3c), while at 22 GPa and 15 W (~2500 K) only ReB_2 was observed. At even higher pressures (22 GPa) and higher temperatures (25 W for each laser, T ~ 4000 K) another set of new reflections was observed. Attempts to index the patterns with known boron phases, including γ-B_{28} and T-B_{192} that according to Parakhonskiy et al. [43] and Oganov et al [44] are the stable boron phases at these conditions were unsuccessful. Therefore, while the presence of at least one further new phase (called

phase B) was unambiguously observed, no lattice parameters could be extracted. All the experimental observations of this study have been summarized in a schematic p–T field shown in Fig. 4.

In order to improve the signal-to-noise ratio we investigated recovered samples at ambient conditions by removing the gaskets from the DAC (Fig. 5). Lattice parameters of phases in the recovered samples are given in Table 1. A typical powder X-ray diffraction pattern from a recovered gasket of a loading that was pressurized up to 21 GPa and heated to ~2500 K is shown in Fig. 5a–b. All phases observed at those (p,T) conditions, ReB_2, Re_3B, and Re_7B_3, and phase A were quenchable. However, it still was not possible to index phase A due to the strong reflection overlap. Also, a typical powder X-ray diffraction pattern from the recovered gasket of the loading that was pressurized up to 22 GPa and heated to ~4000 K is shown in Fig. 5c–d. All phases observed at those (p,T) conditions, ReB_2 and phase B, were quenchable. However, we were still unable to determine the unit cell parameters and a space group. An inspection of the raw diffraction data shows that only very few grains of phase B contributed to the diffraction pattern. Hence, it is likely that numerous weak reflections were unobservable and this severely limits the reliability of the indexing process.

3.2. Bulk and linear compressibilities

The pressure dependencies of the normalized unit cell parameters (X/X_0) of ReB_2, Re_3B and Re_7B_3 are plotted in Figs. 6–8, respectively. Equation-of-state (eos) parameters V_0 (unit cell volume at ambient pressure) and B_0 (isothermal bulk modulus) were

Table 1
Lattice parameters of the phases observed during this study.

| Pressure/GPa, Temperature/K	Phase	a/Å	b/Å	c/Å	V/Å³	Space group
6.4(2)	Re	2.7406(2)	–	4.4389(6)	28.872(4)	P6₃/mmc
Before LH	B2–KCl	3.5845(4)	–	–	46.06(1)	Pm3m
8.9(4)	Re	2.7262(4)	–	4.3967(7)	28.298(7)	P6₃/mmc
Before LH	NaCl	5.2184(7)	–	–	142.11(3)	Fm3m
8.9(4)	ReB₂ᵃ	2.873(1)	–	7.438(5)	53.17(4)	P6₃/mmc
1500	NaCl	5.2184(7)	–	–	142.11(3)	Fm3m
	ReB₂	2.8589(2)	–	7.3911(8)	52.32(1)	P6₃/mmc
8.9(4)	Re₃Bᵇ	2.8507(4)	9.234(1)	7.185(1)	189.14(5)	Cmcm
1500	Re₇B₃ᶜ	7.486(1)	–	4.818(1)	233.83(4)	P6₃mc
	NaCl	5.2546(6)	–	–	145.09(3)	Fm3m
7.6(3)	ReB₂	2.8766(2)	–	7.4421(6)	53.33(1)	P6₃/mmc
1800	Re₇B₃	7.4705(6)	–	4.8420(5)	234.02(3)	P6₃mc
	NaCl	5.2930(5)	–	–	148.29(2)	Fm3m
	ReB₂	2.869(2)	–	7.431(1)	52.99(1)	P6₃/mmc
15.0(4)	Re₃B	2.8783(4)	9.257(1)	7.038(2)	187.52(6)	Cmcm
1500	Re₇B₃	7.4542(3)	–	4.8001(4)	230.98(2)	P6₃mc
	B2–KCl	3.3623(3)	–	–	38.013(5)	Pm3m
22.1(4)	ReB₂	2.8413(3)	–	7.382(1)	51.61(1)	P6₃/mmc
4000	NaCl	4.9819(6)	–	–	123.65(3)	Fm3m
Recovered	ReB₂	2.8823(5)	–	7.436(1)	53.50(1)	P6₃/mmc
ALS	NaCl	5.601(2)	–	–	175.67(9)	Fm3m
	ReB₂	2.8987(3)	–	7.4907(7)	54.506(9)	P6₃/mmc
Recovered	Re₃B	2.9294(3)	9.339(1)	7.144(1)	195.45(5)	Cmcm
ALS	Re₇B₃	7.5331(8)	–	4.8575(7)	238.72(5)	P6₃mc
	B1–KCl	6.2950(9)	–	–	249.45(6)	Fm3m
Recovered	ReB₂	2.8788(4)	–	7.4345(4)	53.359(4)	P6₃/mmc
PETRA III	Re₇B₃	7.462(1)	–	4.842(1)	233.50(8)	P6₃mc
	B1–KCl	6.251(1)	–	–	244.29(8)	Fm3m

ᵃ In ReB₂, Re is located on 1/3, 2/3, 1/4 (2c) and B on 1/3, 2/3, 0.548 (4f) [7].

ᵇ In Re₃B, Re is located on 0, 0.135, 0.062 (8f) and 0, 0.426, 1/4 (4c) while B on 0, 0.744, 1/4 (4c) [7].

ᶜ In Re₇B₃, Re is located on 1/3, 2/3, 0.068 (2b); 0.122, 0.878, 1/4 (6c) and 0.544, 0.456, 0.068 (6c) while B on 0.813, 0.187, 0.33 (6c) [7].

determined by a least-squares fit to a 2nd-order Birch–Murnaghan equation of state (BM-eos) using the program EOS-FIT [45]. The pressure-volume (p–V) data were weighted with the experimental errors of the pressures and volumes. The parameters obtained from all the eos fits are summarized in Table 2.

For ReB₂ bulk moduli of $B_{\text{ReB}_2} = 360$–382 GPa have been reported [6], and hence ReB₂ is among the least compressible TM-boride phases studied so far, but significantly more compressible than OsB (431–453 GPa) and Os₂B₃ (396–443 GPa). The bulk modulus of ReB₂ obtained from experiment in the present study $B_{\text{ReB}_2} = 360(18)$ GPa agrees within the experimental error with the values reported earlier. However, the 3rd-order Birch–Murnaghan equation of state reported by Levine et al. [46] does not describe our compression data well, with increasing discrepancies appearing with increasing pressure. Regrettably, the volume data was not published in the earlier study and hence the role of the unusually low pressure derivative of $B' = 0.84$ obtained by Levine et al. [46] couldn't be evaluated by us. Our DFT-based calculations (see below) however strongly suggest that B' should be close to 4 instead.

In the present study, the bulk moduli of Re₃B and Re₇B₃ have been determined for the first time. The bulk modulus of Re₃B, $B_{\text{Re}_3\text{B}} = 320(15)$ GPa (Table 2, Fig. 7) is similar to those of transition metal borides like ZrB₂ (317 GPa), VB₂ (322 GPa) and TaB₂ (336 GPa) [6]. In contrast, the experimentally determined bulk modulus of Re₇B₃, $B_{\text{Re}_7\text{B}_3,\exp} = 438(16)$ GPa (Table 2, Fig. 8) is very similar to those of ultra-incompressible OsB or Os₂B₃.

We complemented the experimental studies by DFT-based atomistic model calculations and calculated the compression behavior and 3rd-order BM equation of states and employed stress-strain calculations to derived elastic properties such as elastic
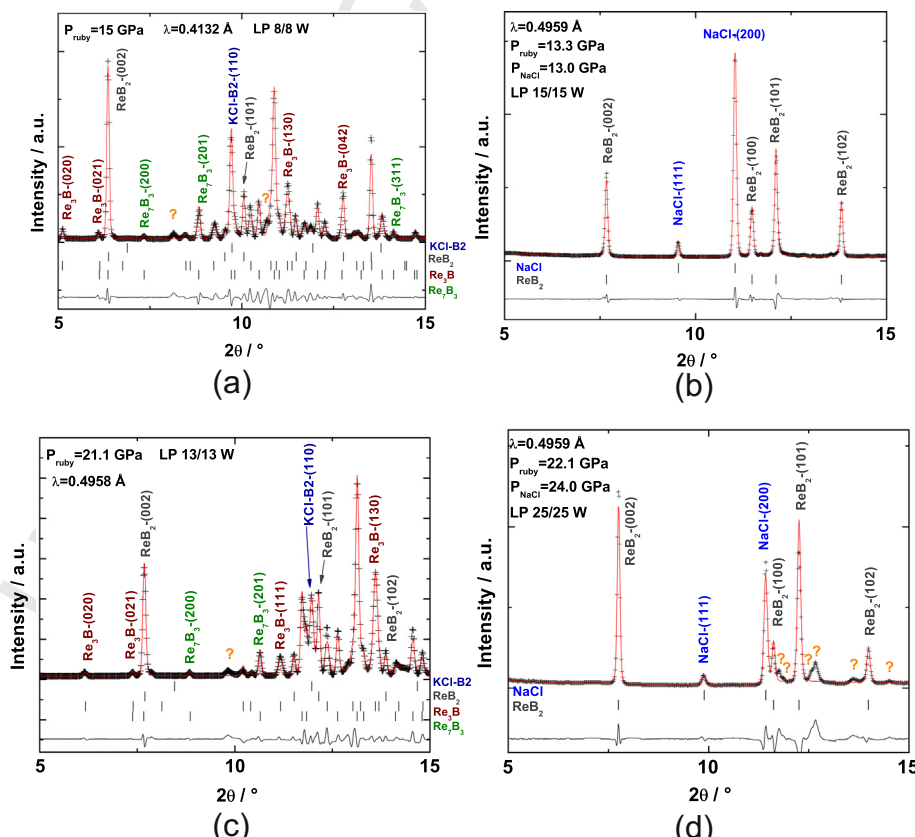

Fig. 3. High pressure powder X-ray diffraction patterns after laser heating. Question marks indicate unindexed reflections. Panels (a, c) and (d) show the presence of phase A and phase B, respectively.
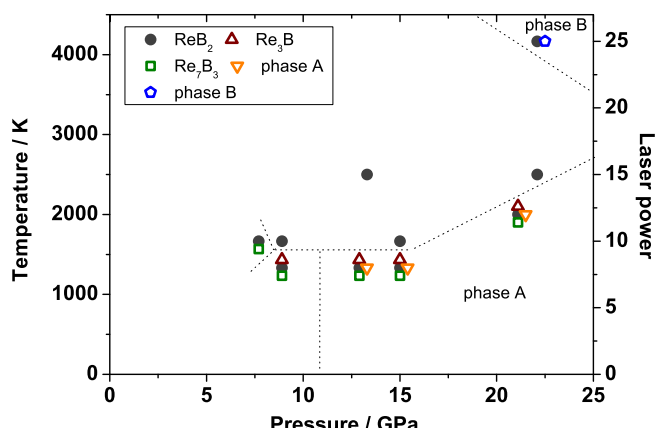
Fig. 4. Schematic p–T field of the phases observed during the reaction of rhenium and boron from the elements in a laser heated diamond anvil cell. The lines are only guides to the eye.

stiffness coefficients c_{ij}, bulk modulus B, shear modulus G and Young modulus Y. The results are given in Table 3. We obtained theoretical compression data which were fitted using 2nd- and 3rd-order BM eos (Table 2). For all 3rd-order BM eos fits B' was close to 4 ($B'_{ReB_2} = 4.1(4)$, $B'_{Re_3B} = 4.4(4)$, $B'_{Re_7B_3} = 4.4(4)$) and hence bulk moduli were obtained using a 2nd-order BM-eos.

As has been mentioned above, ReB_2 is one of the most studied TM-borides. The DFT-value for the bulk modulus derived from a eos agrees within 5% with our experimental value, but in contrast to an earlier study [46] we obtain a $B' = 4.1(4)$. The bulk modulus derived
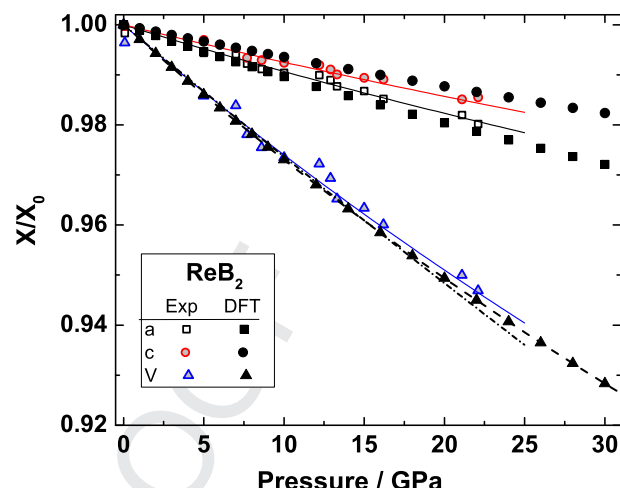
Fig. 6. Pressure dependencies of the normalized unit cell volume and lattice parameters of ReB_2. The values of the bulk modulus can be found in Table 2. The solid lines represent best fits of 2nd-order Birch–Murnaghan equations of state, while the dashed line represents the eos obtained by DFT. The dash-dot line represent the eos reported by Ref. [46].

from stress-strain calculations agrees with the eos-based value. The values for the c_{ij} obtained here from stress-strain calculations for ReB_2 and Re_7B_3 agree with those obtained earlier by DFT calculations [27,32,47]. It is worth to mention that the agreement is good although these calculations were performed with other functionals, other pseudopotentials and other DFT-implementations. The value obtained here for the Vickers hardness Hv of ReB_2 agrees with those

(a)

(b)

(c)

(d)
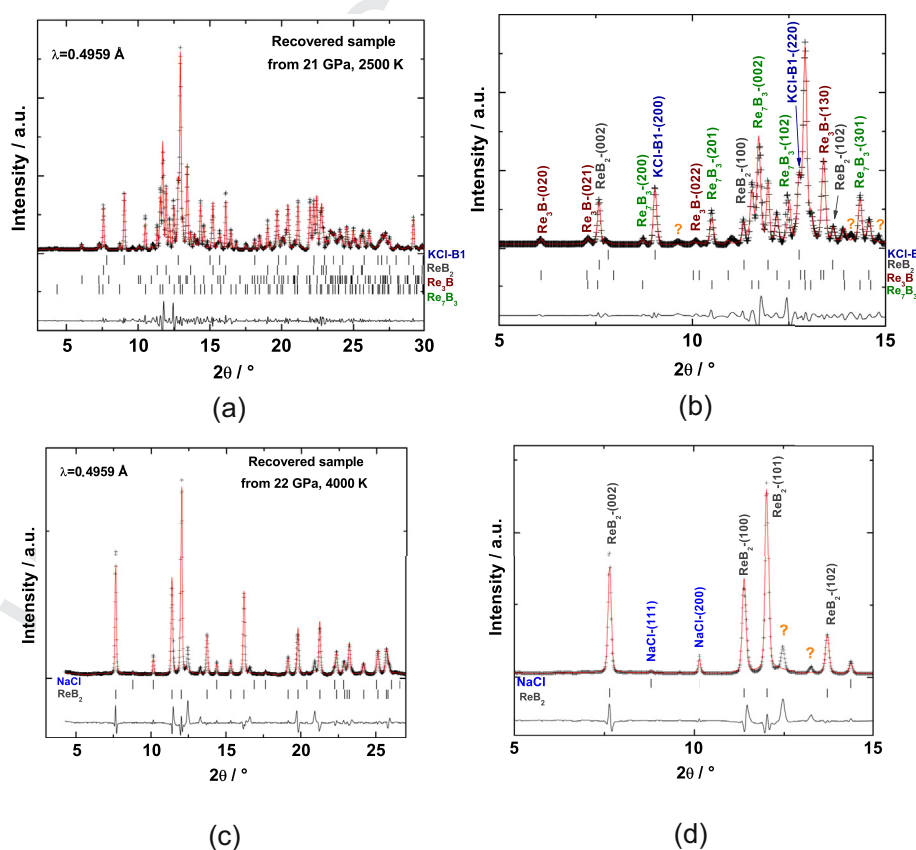
Fig. 5. Powder diffraction patterns from the recovered gaskets. Full range (a,c) and enlargements (b,d) of the same powder diffraction pattern demonstrating the high quality of the fits.
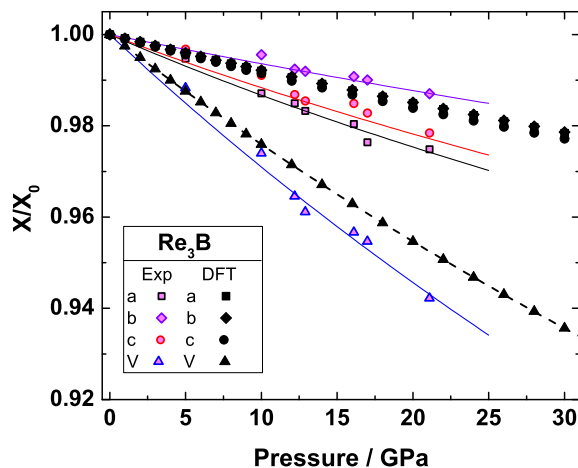
Fig. 7. Pressure dependencies of the normalized unit cell volume and lattice parameters of Re_3B. The values of the bulk modulus can be found in Table 2. The solid lines represent best fits of 2nd-order Birch−Murnaghan equations of state.

reported earlier. Fig. 6 demonstrates that the linear compressibilities are very well reproduced. Due to the good agreement between the DFT model and experimental data, including a state-of-the-art neutron powder diffraction study [48], we believe our model is reliable.

For Re_3B, the agreement between the model calculations and the experimental data is significantly poorer. Fig. 7 shows that the compressibility is significantly underestimated, yielding a too high value for *B*, and the significant anisotropy of the linear compressibilities is also not reproduced well. For Re_3B, despite very tight convergence parameters, our calculations indicated a negative value for $c_{44} \approx -76$ GPa, i.e. the model structure is elastically unstable. This instability has also been computed by Gou et al. [27]. It is worthwhile to note that while for all other borides investigated here the computed lattice parameters agree to better than 1% with the experimental value, with the exception of one lattice parameter of Re_3B where the difference is still reasonable 2.3%. This implies that probably Re_3B is stabilized by defects or impurities. While for ReB_2 a modern neutron powder diffraction study has been presented, with which the boron atoms can be located unequivocally [48], the structure of Re_3B has not been studied by neutron diffraction. In the initial studies by Aronsson et al. [20,21] the boron
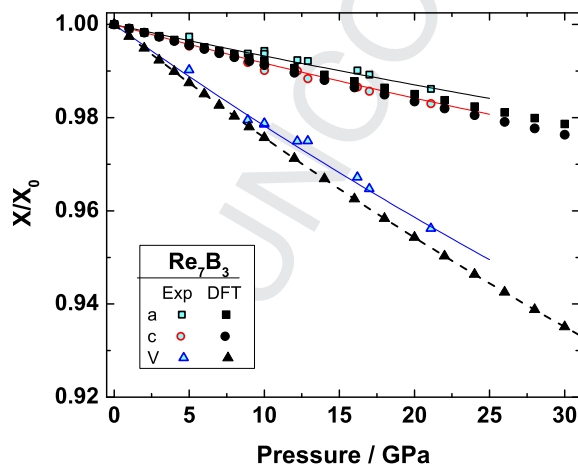

Fig. 8. Pressure dependencies of the normalized unit cell volume and lattice parameters of Re_7B_3. The values of the bulk modulus can be found in Table 2. The solid lines represent best fits of 2nd-order Birch−Murnaghan equations of state, while the dashed line represents the eos obtained by DFT.

Table 2
Equation of state parameters from fits of 2nd-order Birch−Murnaghan equation of state to the experimental data and corresponding values from DFT−GGA model calculations. Pure rhenium ($a_{exp} = 2.7812(1)$ Å, $c_{exp} = 4.4612(1)$ Å [49]) is also reproduced well by the DFT model calculations ($a_{DFT} = 2.7712$ Å, $c_{DFT} = 4.4814$ Å).

			ReB_2	Re_3B	Re_7B_3
a	[Å]	Exp	2.899(1)	2.931(2)	7.537(2)
		DFT	2.9068	2.9019	7.5311
b	[Å]	Exp	–	7.155(8)	–
		DFT	–	7.3278	–
c	[Å]	Exp	7.493(3)	9.343(6)	4.855(2)
		DFT	7.4878	9.3874	4.9018
V_0	[Å³]	Exp	54.5(3)	195.8(3)	238.9(2)
		DFT eos	54.792(2)	196.06(1)	241.18(3)
B_0	[GPa]	Exp	360(18)	320 (15)	438 (16)
		Exp[a]	371	–	–
		DFT eos	346(1)	389(1)	385(1)
		DFT C_{ij}	345(1)	$c_{44} < 0$	385(1)
K_{a0}	[GPa]	Exp	336(12)	230(11)	474(15)
		DFT	288.0(3)	385.1(3)	386(1)
K_{b0}	[GPa]	Exp	–	265(20)	–
		DFT	–	387(2)	–
K_{c0}	[GPa]	Exp	424(19)	500(40)	381(19)
		DFT	484(1)	350.7(6)	346(3)

[a] From 3rd order BM-eos with a $B' = 0.84$ [46].

atoms were not located, and instead assumed to be located on a Wykoff position 4(c). Also, the composition was not verified. Therefore, this structure has to be re-evaluated.

For Re_7B_3, the compressibility is overestimated by 13%, and the anisotropy of the linear compressibilities is reproduced only moderately well (Fig. 8). The discrepancy between experiment and theory is reasonable for the lattice parameters at ambient conditions. The DFT data are internally consistent, as the bulk modulus obtained from stress-strain calculations is in very good agreement with the value obtained from the eos. An LDA-based calculation [32] gave c_{ij} values similar to those observed here, and a theoretical bulk modulus of 404 GPa, which, as expected, is slightly larger than the WC-GGA value (385 GPa) obtained in the present study. A PBE-GGA value computed by Ref. [27] is slightly lower (378 GPa), which is also expected according to experience [33,15]. In contrast to the results for Re_3B, for Re_7B_3 the DFT model is elastically stable.

4. Conclusions

We have identified the occurrence of new Re−B phases at high-(*p, T*) conditions. The limitations of DAC-based diffraction studies precluded the unambiguous determination of the lattice parameters of these phases. It is worthwhile to note that in none of the studies aimed at predicting properties of phases in the Re−B system (e.g. Refs. [27,32]) a phase with lattice parameters close to those observed for the new phases here has been reported. We show that these phases can be recovered. Hence, it should be possible to synthesize larger amounts of at least phase A, as the

Table 3
Elastic stiffness coefficients C_{ij}, bulk modulus B, shear modulus G, Young modulus Y and empirical microhardness Hv from DFT−GGA calculations. All values are given in GPa. The ReB_2 data are in good agreement with values published earlier by Ref. [47].   **Q2**

Phase	C_{11}	C_{33}	C_{44}	C_{12}	C_{13}	B	G	Y	Hv
ReB_2	646(2)	1029(3)	265.3(5)	157(1)	119.7(5)	335(1)	283	599[a], 993	44.7[b]
Re_3B[c]	641(2)	612(4)	−76(38)	–	–	389(1)	157	481, 445, 447	25.5
Re_7B_3	630(5)	590.1(5)	133(4)	262(1)	273(1)	385(1)	159	466[a], 422	24.1

[a] Same value for *x*-axis and *y*-axis.
[b] Values reported earlier: 43 [41], 30−48 [6].
[c] $C_{222} = 617(4)$, $C_{555} = 261.2(4)$, $C_{666} = 247.9(3)$, $C_{712} = 272(2)$, $C_{813} = 263(1)$, $C_{1223} = 281(1)$.

7

required (p, T)-conditions can be achieved in large volume multi anvil high pressure devices. Such studies are now planned.

While our finding that Re_7B_3 is extremely incompressible is very robust, the associated error is quite large. However, Re_7B_3 can also be obtained by arc melting [22] and hence it is now worthwhile to synthesize and check a phase pure sample at ambient pressure, and then pressurize this sample in order to corroborate our findings and increase the precision of the bulk modulus.

We also think that a careful compositional and structural study of Re_3B is of interest in order to elaborate the likely role of defects in the stabilization of this compound.

With respect to superhard phases, Levine et al. [46] argued that ReB_2 is probably the hardest rhenium boride. Our calculations of the elastic stiffness coefficients (Table 3), and consequently of the shear moduli, of the rhenium borides allow us to quantify their conclusions. The shear modulus is linearly correlated with the hardness of many binary compounds [46]. From our calculations, ReB_2, with its high shear modulus of 283 GPa, should have a hardness of about 40–45 GPa, and this is what has been observed experimentally. Re_7B_3, although more incompressible than ReB_2, has a shear modulus of 159 GPa, which is only about half of that of ReB_2, and consequently here we predict a hardness of about 24 GPa only.

Acknowledgments

References

[1] Q. Gu, G. Krauss, W. Steurer, Transition metal borides: superhard versus ultra-incompressible, Advanced Materials 20 (2008) 3620–3626.

[2] S. Otani, T. Aizawa, Y. Ishizawa, Preparation of ReB_2 single crystals by the floating zone method, Journal of Alloys and Compounds 252 (1997) L19–L21.

[3] R.G. Munro, Material properties of titanium diboride, Journal of Research of the National Institute of Standards and Technology 105 (2000) 709–720.

[4] E. Opila, S. Levine, J. Lorincz, Oxidation of ZrB_2-and HfB_2-based ultra-high temperature ceramics: effect of Ta additions, Journal of Materials Science 39 (2004) 5969–5977.

[5] Y.D. Blum, J. Marschall, D. Hui, B. Adair, M. Vestel, Hafnium reactivity with boron and carbon sources under non-self-propagating high-temperature synthesis conditions, Journal of the American Ceramic Society 91 (2008) 1481–1488.

[6] A. Friedrich, B. Winkler, E.A. Juarez-Arellano, L. Bayarjargal, Synthesis of binary transition metal nitrides, carbides and borides from the elements in the laser-heated diamond anvil cell and their structure–property relations, Materials 4 (2011) 1648–1692.

[7] ICSD, National Institute of Standards and Technology Gaitersburg, Inorganic Crystal Structure Database. ICSD Release 2012/2, Fachinformationszentrum Karlsruhe, 2012.

[8] B. Yao, L. Liu, J. Chen, B.Z. Ding, W.H. Su, The effect of pressure on the phase transition of Fe_3B to $_2B$, Journal of Physics D: Applied Physics 31 (1998) 790–793.

[9] J.F. Cannon, P.B. Farnsworth, High pressure syntheses of $ThB12$ and HfB_{12}, Journal of the Less Common Metals 92 (2) (1983) 359–368.

[10] A.S. Pereira, C.A. Perottponi, J.A.H. da Jornada, J.M. Léger, J. Haines, Compressibility of AlB_2-type transition metal diborides, Journal of Physics: Condensed Matter 14 (2002) 10 615–10 618.

[11] A. Yamamoto, C. Takao, T. Masui, M. Izumi, S. Tajima, High-pressure synthesis of superconducting $Nb_{1-x}B_2$ ($x = 0$–0.48) with the maximum $T_c = 9.2$ K, Physica C 383 (2002) 197–206.

[12] B. Chen, D. Penwell, J.H. Nguyen, M.B. Kruger, High pressure X-ray diffraction study of Fe_2b, Solid State Communications 129 (9) (2004) 573–575.

[13] R.W. Cumberland, M.B. Weinberger, J.J. Gilman, S.M. Clark, S.H. Tolbert, R.B. Kaner, Osmium diboride, an ultra-incompressible, hard material, Journal of the American Chemical Society 127 (2005) 7264–7265.

[14] Q.F. Gu, G. Krauss, F. Gramm, W. Steurer, On the compressibility of TiC in microcrystalline and nanoparticulate form, Journal of Physics: Condensed Matter 20 (2008) 445226.

[15] B. Winkler, E.A. Juarez-Arellano, A. Friedrich, L. Bayarjargal, F. Schröder, J. Biehler, V. Milman, S.M. Clark, J. Yan, In situ synchrotron X-ray diffraction study of the formation of $TaB2$ from the elements in a laser heated diamond anvil cell, Solid State Science 12 (2010) 2059–2064.

[16] H.Y. Chung, M.B. Weinberger, J.B. Levine, A. Kavner, J.M. Yang, S.H. Tolbert, R.B. Kaner, Synthesis of ultra-incompressible superhard rhenium diboride at ambient pressure, Science 316 (2007) 436–439.

[17] S. La Placa, B. Post, The crystal structure of rhenium diboride, Acta Crystallographica 15 (1962) 97.

[18] J.B. Levin, S.J. Nguyen, H.I. Rasool, J.A. Wright, S.E. Brown, R.B. Kaner, Preparation and properties of metallic, superhard rhenium diboride crystals, Advanced Functional Materials 130 (2008) 16953–16958.

[19] A. Latini, J.V. Rau, D. Ferro, R. Teghil, V.R. Albertini, S.M. Barinov, Superhard rhenium diboride films: preparation and characterization, Chemistry of Materials 20 (2008) 4507–4511.

[20] B. Aronsson, M. Bäckman, S. Rundqvist, The crystal structure of Re_3B, Acta Chemica Scandinavica 14 (1960) 1001–1005.

[21] B. Aronsson, E. Stenberg, J. Aselius, Borides of rhenium and the platinum metals. The crystal structures of Re_7B_3, Re_3B, Rh_7B_3, $RhB_{1.1}$, $IrB_{1.1}$, PtB, Acta Chemica Scandinavica 14 (1960) 733–741.

[22] A. Kawano, Y. Mizuta, H. Takagiwa, T. Muranaka, J. Akimitsu, The superconductivity in Re–B system, Journal of the Physical Society of Japan 72 (2003) 1724–1728.

[23] H. Takagiwa, A. Kawano, Y. Mizuta, T. Yamamoto, M. Yamada, K. Ohishi, T. Muranaka, J. Akimitsu, W. Higemoto, R. Kadono, Magnetic penetration depth of a new boride superconductor Re_3B, Physica B 326 (2003) 355–358.

[24] R.F. Zhang, S. Veprek, A.S. Argon, Mechanical and electric properties of hard rhenium diboride of low elastic compressibility studied by first-principles calculation, Applied Physics Letters 91 (2007) 201914.

[25] W. Zhou, H. Wu, T. Yildirim, Electronic, dynamical, and thermal properties of ultra-incompressible superhard rhenium diboride: a combined first-principles and neutron scattering study, Physical Review B 76 (2007) 184113.

[26] G. Soto, M.G. Moreno-Armenta, A. Reyes-Serrato, Study on the formation of rhenium borides by density functional calculations, Computational Materials Science 44 (2008) 628–634.

[27] H. Gou, Z. Wang, J. Zhang, S. Yan, F. Gao, Structural stability and elastic and electronic properties of rhenium borides: first principle investigations, Inorganic Chemistry 48 (2009) 581–587.

[28] F. Peng, Q. Liu, H. Fu, X. Yang, Electronic and thermodynamic properties of ReB_2: under high pressure and temperature, Solid State Communications 149 (2009) 56–59.

[29] A. Šimůnek, Anisotropy of hardness from first principles: the cases of ReB_2: and osb_2, Physical Review B 80 (2009) 060103.

[30] E. Zhao, J. Wang, J. Meng, Z. Wu, Ab initio study on the electronic and mechanical properties of reb and rec, Journal of Solid State Chemistry 182 (2009) 960–965.

[31] O.J. Žogał, Z. Fujod, P. Herzig, A. Pietraszko, A.B. Lyashchenko, S. Jurga, V.N. Paderno, Crystal structure, electric field gradient, and electronic charge densities in reb_2: a single crystal X-ray, Í1b nuclear magnetic resonance, and first-principles study, Journal of Applied Physics 106 (2009) 033514.

[32] E. Zhao, J. Wang, J. Meng, Z. Wu, Phase stability and mechanical properties of rhenium borides by first-principles calculations, Journal of Computational Chemistry 31 (July 2010) 1904–1910.

[33] E.A. Juarez-Arellano, B. Winkler, A. Friedrich, L. Bayarjargal, V. Milman, J. Yan, S.M. Clark, Stability field of the high-(P, T) Re_2C phase and properties of an analogous osmium carbide phase, Journal of Alloys and Compounds 481 (2009) 577–581.

[34] H. Mao, P. Bell, J. Shaner, D. Steinberg, Specific volume measurements of Cu, Mo, Pd, and Ag and calibration of the ruby R1 fluorescence pressure gauge from 0.06 to 1 Mbar, Journal of Apply Physics 49 (1978) 3276–3283.

[35] A.P. Hammersley, S.O. Svensson, M. Hanfland, A.N. Fitch, D. Hauserman, Two-dimensional detector software: from real detector to idealised image or two-theta scan, High Pressure Research 14 (1996) 235–248.

[36] K. Syassen, Datlab. Version 1.37d, MPI/FKF Stuttgart, Germany, 2005.

[37] J. Rodriguez-Carvajal, Recent advances in magnetic structure determination by neutron powder diffraction, Physica B 192 (1993) 55–69.

[38] S.J. Clark, M.D. Segall, C.J. Pickard, P.J. Hasnip, M.J. Probert, K. Refson, M.C. Payne, First principles methods using CASTEP, Zeitschrift für Kristallographie 220 (2005) 567–570.

[39] Z. Wu, R.E. Cohen, More accurate generalized gradient approximation for solids, Physical Review B 73 (2006) 235116.

[40] H. Monkhorst, J.D. Pack, Special points for Brillouin-zone integrations, Physical Review B 13 (1976) 5188–5192.

[41] A.L. Ivanovskii, Microhardness of compounds of rhenium with boron, carbon and nitrogen, Journal of Superhard Materials 34 (2012) 75–80.

[42] A.J. Campbell, D.L. Leinz, Compression of KCl in the B_2 structure to 56 GPa, Journal of Physics and Chemistry of Solids 52 (1991) 495–499.

891
892
893

[43] G. Parakhonskiy, N. Dubrovinskaia, E. Bykova, R. Wirth, L. Dubrovinsky, Experimental pressure-temperature phase diagram of boron: resolving the long-standing enigma, Scientific Report vol. 1 (2011) 96.

894
895
896

[44] A.R. Oganov, J. Chen, C. Gatti, Y. Ma, Y. Ma, C.W. Glass, Z. Liu, T. Yu, O.O. Kurakevych, V.L. Solozhenko, Ionic high-pressure form of elemental boron, Nature 457 (2009) 863–867.

[45] R.J. Angel, EOS-FIT, Version 5.2, Virginia Tech, Blacksburg, U.S.A, 2001.

897
898

[46] J.B. Levine, S.H. Tolbert, R.B. Kaner, Advancements in the search for superhard ultra-incompressible metal borides, Advanced Functional Materials 19 (2009) 3519–3533.

899
900
901
902

[47] Y.X. Wang, Elastic and electronic properties of tcb_2 and superhard reb_2: first-principles calculations, Applied Physics Letters 91 (2007) 101904.

[48] M. Frotscher, M. Hölzel, B. Albert, Crystal structures of the metal diborides reb_2, rub_2, and osb_2 from neutron powder diffraction, Zeitschrift für Anorganische und Allgemeine Chemie 636 (2010) 1783–1786.

903
904
905
906

[49] E.A. Juarez-Arellano, B. Winkler, A. Friedrich, D.J. Wilson, M. Koch-Müller, K. Knorr, S.C. Vogel, J.J. Wall, H. Reiche, W. Crichton, M. Ortega-Aviles, M. Avalos-Borja, Reaction of rhenium and carbon at high pressures and temperatures, Zeitschrift für Kristallographie 223 (2008) 492–501.